Design Principles of Dual-Functional Molecular Switches in Solid-

State Tunnel Junctions

Damien Thompson¹*, Enrique del Barco²*, and Christian A. Nijhuis^{3,4}*

- ¹ Department of Physics, Bernal Institute, University of Limerick, Limerick V94 T9PX, Ireland
- ² Department of Physics, University of Central Florida, Orlando FL 32816 USA
- ³ Department of Chemistry, National University of Singapore, 3 Science Drive 3, Singapore 117543, Singapore
- ⁴ Centre for Advanced 2D Materials and Graphene Research Centre, National University of Singapore, 6 Science Drive 2, Singapore 117546, Singapore.
- *Correspondence to: chmnca@nus.edu.sg, damien.thompson@ul.ie, and delbarco@ucf.edu

Abstract

Molecular electronics has improved tremendously over the past twenty years, but it remains challenging to develop molecular switches that operate well in two-terminal tunnel junctions. Emerging technologies demand multifunctional junctions that can switch between different operations within a single molecule or molecular monolayer. Usually the focus is placed on molecules that shift the junctions between high and low conductance states, but here we describe molecular junctions with dual-functional switching capability. We discuss the operating mechanism of such switches and present examples of "two-in-one" junctions of a diode placed in series with an additional switch, which can operate either as an electrostatic or a memory on/off switch. We propose guidelines for future designs of such dual-function molecular switches and provide an outlook for future directions of research.

Introduction

Electrically driven switches are the cornerstone of electrical circuitry, and the continued drive for device miniaturization, particularly in upcoming technologies such as neuromorphic computing and biomedical and soft electronics, motivates the development of efficient molecular switches that can reduce the footprint of devices, decrease power consumption, and enable complementary functionalities to existing solutions. 1,2,3,4 While the last two decades of intense experimental and theoretical research has brought molecular electronics to the point where it is now possible to routinely measure charge transport across self-assembled monolayer and single molecule tunnel junctions, 5,6,7,8,9,10 it is still challenging to address molecular switches in solid-state junctions despite the fact that solution-based (multi-functional) molecular switches are readily available. 11,12,13,14,15 In this Progress Article, we outline the design principles of dual-functional molecular switches in solid-state junctions that could greatly simplify electronic circuity, and we identify the eulprits-pitfalls and challenges in obtaining efficient switching. We show how well-crafted dual-functional molecular switches can mimic complex electronic function in solid state tunnel junctions that is otherwise only achievable with relatively comparatively complex CMOS based architectures.

Molecular switches operate well in solution or in the form of monolayers exposed to solution, and require external stimuli, *e.g.*, light, magnetic field, ion binding, heat, or changes in pH or electrochemical potential, to toggle between two, or more, states. ^{13,14,16,17,18,19,20,21,22} These states are usually different redox, conformational, or magnetic states, which are readily accessible in solution and can be read-out with conventional spectroscopy, electrochemical techniques, or magnetic measurements. By contrast, in solid-state two-terminal junctions the mechanisms to stabilize the different molecular states of the switches are not readily available: the conformational degree of freedom is much smaller than in solution (due to steric hindrance), lack of electrolyte (especially important to stabilize different redox-states), and excited states

(especially particularly for light-triggered switches) may be quenched. Consequently, most molecular switches in molecular junctions yield low conduction on/off ratios (<10) or suffer from slow switching speeds on the order of 10^2 - 10^3 s, 23,24,25,26,27,28,29,30 apart from a few exceptions in which stochastic switching remains an issue^{31,32}. Thus, molecular switches are required that are specifically designed to change the conductance of two-terminal junctions so that the on and off states are stabilized.

Operation Principles. Biological molecular evolution features a class of multi-functional proteins in which the originally selected enzymatic role becomes over time augmented with additional regulatory roles in, for example, iron regulatory protein.³³ Inspired by this concept of multi-functionality, we seek to build-in additional functionality to developed circuit elements. In the context of molecular electronics, molecular switches toggle the junction between a high (on) and low (off) current state. So far, efforts have focused on such monofunctional junctions with a variety of molecules including photo-active switches, 24,26,34,35 redox-active molecules, ^{28,27,31,25,32,36} bond topology switching, ^{37,38} and spin switches ^{21,39,40,41}. These approaches usually only work well at low temperatures because at room temperature the on state is not stable and the molecule thermalizes back to the original state. In this perspective, we go one step further and introduce a dual-functional molecular switch specifically tailored to realize molecular junctions that toggle between two different functionalities at room temperature. For practical reasons, it is desirable to achieve switching in large-area molecular junctions (because of their stability) and to use differences in applied bias voltage $\sqrt{V_7}$ (rather than external stimili) to induce switching and to read out the on and off states of the junction rather than external stimili. 8, 42, 43 Figure 1 shows two possible ways to induce large conductance switching in junctions by changing the tunneling barrier height and the molecule—electrode coupling, Γ. In this example, the highest occupied molecular orbital,

HOMO, is lower in energy than the Fermi-level, $E_{\rm f}$, of the electrodes, as indicated by $\delta_{\rm EM}$, but a similar reasoning applies to junctions where the lowest unoccupied molecular orbital, LUMO, is shifted above $E_{\rm f}$. The tunneling barrier height is given by $\delta_{\rm EM}$ and the coupling strength of the molecular orbital with the left (l) and right (r) electrodes are given by $\Gamma = \Gamma_1 + \Gamma_r$. In the Landauer framework for coherent tunneling, ^{44,45} the current across the junction, I, is given by

$$I = \frac{2e}{h} \int_{-\infty}^{\infty} T(E) \left[f_l(E) - f_r(E) \right] dE$$
 1a

with

$$T = \frac{4\Gamma_l \Gamma_r}{(E - \varepsilon)^2 + [\Gamma_l + \Gamma_r]^2}$$
 1b

and

$$\varepsilon = \mu_r(V) + \delta_{ME} + \eta eV$$
 10

where e = charge of the electron, h = Planck's constant, T(E) = transmission function as a function of energy (E), f(E) = Fermi distribution function, $\mu_r(V)$ = the electrochemical potential of the right electrode and $\eta = V_r/(V_l + V_r)$ is the dimensionless voltage division parameter giving the ratio of the voltage drop between the molecule and the right electrode with respect to the total voltage drop in the junction. Figure 1a shows the junction in the initial state when no external voltage bias is applied (V = 0 V). In this situation, the junction is in the off state (low conductance state) with the HOMO energetically well below E_f as given by $\delta_{\rm EM,off}$ and weak molecule—electrode interaction $\Gamma_{\rm off}$ where off resonant tunneling (of holes) dominates the mechanism of charge transport. Figure 1b shows the same junction in the on state (high conductance state) where under the action of applied bias a hole is injected into the HOMO resulting in a semi-occupied molecular orbital (SOMO) with the following two changes yielding an increase in conduction: i) the tunneling barrier height decreases $\delta_{\rm EM,on} < \delta_{\rm EM,off}$ and ii) the molecule—electrode coupling strength increases $\Gamma_{\rm on} > \Gamma_{\rm off}$ (which results in broadening of the molecular orbital as schematically indicated). Note that the same effect would be achieved by an increase in just one of the molecule-electrode couplings $(\Gamma_i$ or Γ_r), as

the lowest coupling limits the conductance, without resulting in an measurable change of the level width (which is determined as the addition of bothby $\Gamma_l + \Gamma_r$). In principle, the relative values of Γ_l and Γ_r can change upon switching making it possible to control the asymmetry of the junction and change, *e.g.*, diode functionality. In the following sections we discuss in detail how changes in both δ_{EM} and Γ can be used to obtain dual-functional switches, through two examples. On a final note, charging of the molecule will likely result in other effects as well and induce, *e.g.*, mirror charges in the electrodes (and associated renormalization of energy levels) or changes in the potentials drops across the junction. ^{46,47,48,49,50,51} Such effects are important to consider and potentially could even be exploited to enhance electronic functionalities.

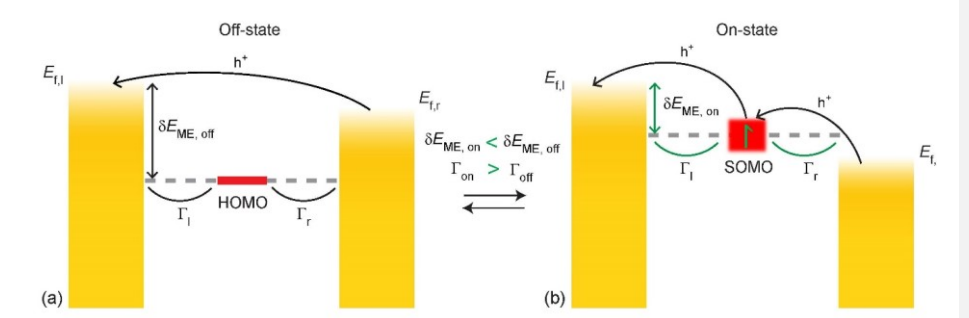


Figure 1: Energy level diagrams with a junction in the off (a) and on state (b) illustrating the operation mechanism of dual-functional molecular junctions as explained in detail in the text. The yellow rectangles indicate the filled states of the electrodes. The black arrows indicate the change in the mechanism of hole transport, the double black and green arrows indicate in the change in $\delta_{\rm EM}$, and the black and green arcs indicate the changes in Γ and associated broadening of the molecular level (red bar).

Diode in series with on/off switch. To demonstrate that this operation principle works, Figure 2a shows the schematic illustration of a dual-functional junction with a monolayer of

Formatted: Font: Italic

S(CH₁₅)FcC=CFc (Fc = ferrocene) that behaves as a molecular diode (Fig. 2b) in series with an electrostatic on/off switch, and Table 1 summarizes the operating parameters.⁵² The long alkyl spacer ensures that the FcC \equiv CFc (in shorthand, Fc₂) functionality is decoupled from $E_{\rm f,l}$ so it follows the changes in $E_{\rm f,r}$ under applied bias because $\eta = 0.95$ (most the potential drops along the alkyl chain between the HOMO and the left electrode). Only at negative bias (Fig. 2c-d), the HOMO falls in the conduction window and a hole can be injected in each Fc unit. At positive bias the HOMO falls outside the conduction window and does not participate in the mechanism of charge transport. 4843,53,54 This change in the mechanism of charge transport (black arrows in Fig. 2c-d) results in typical rectification ratios RR = 100-500 which are very close to the maximum values of R of 10³ expected for single-level molecular junctions operating in the Landauer regime (indicated by the dashed red line in Fig. 2b). These RR values, however, are orders of magnitude lower than RR values from diodes based on Schottky barriers or pn-junctions and therefore a mechanism to "break" the Landauer limit is needed. 55 Charge can be injected in the redox-active Fc groups but only the HOMO falls inside the conduction window at negative bias. Therefore, the Fc—top electrode interaction changes from a relatively weak van der Waals (vdW) to a strong Coulombic interaction (green double arrow in Fig. 2cd). In addition, electrostatic repulsions between neighboring (Fc₂)²⁺ units result in an expansion of the monolayer as visualized and quantified with molecular dynamics simulations (Fig. 2e). These two effects result in a large increase in the number of molecules contributing to conduction through the junction only in one direction of bias, enhancing the performance of the molecular diode by a factor of 1000. Accounting for this change in the number of conducting molecules inside the junctions in the Landauer model, 4944 a good fit with the experimental data was obtained (solid red line in Fig. 2b). In this example two functionalities were achieved as follows: i) controlling $\delta_{\rm EM}$ and Γ_1 ensures charge injection occurs in only one direction of bias to achieve diode functionality, and i) controlling Γ_r via electrostatic

interactions by changing the polarity of the applied bias to achieve an on/off switch functionality. In other words, the diode functionality was enhanced by an in-series electrostatic on/off switch as <u>indicated</u> schematically <u>indicated</u> in Fig. 2a.

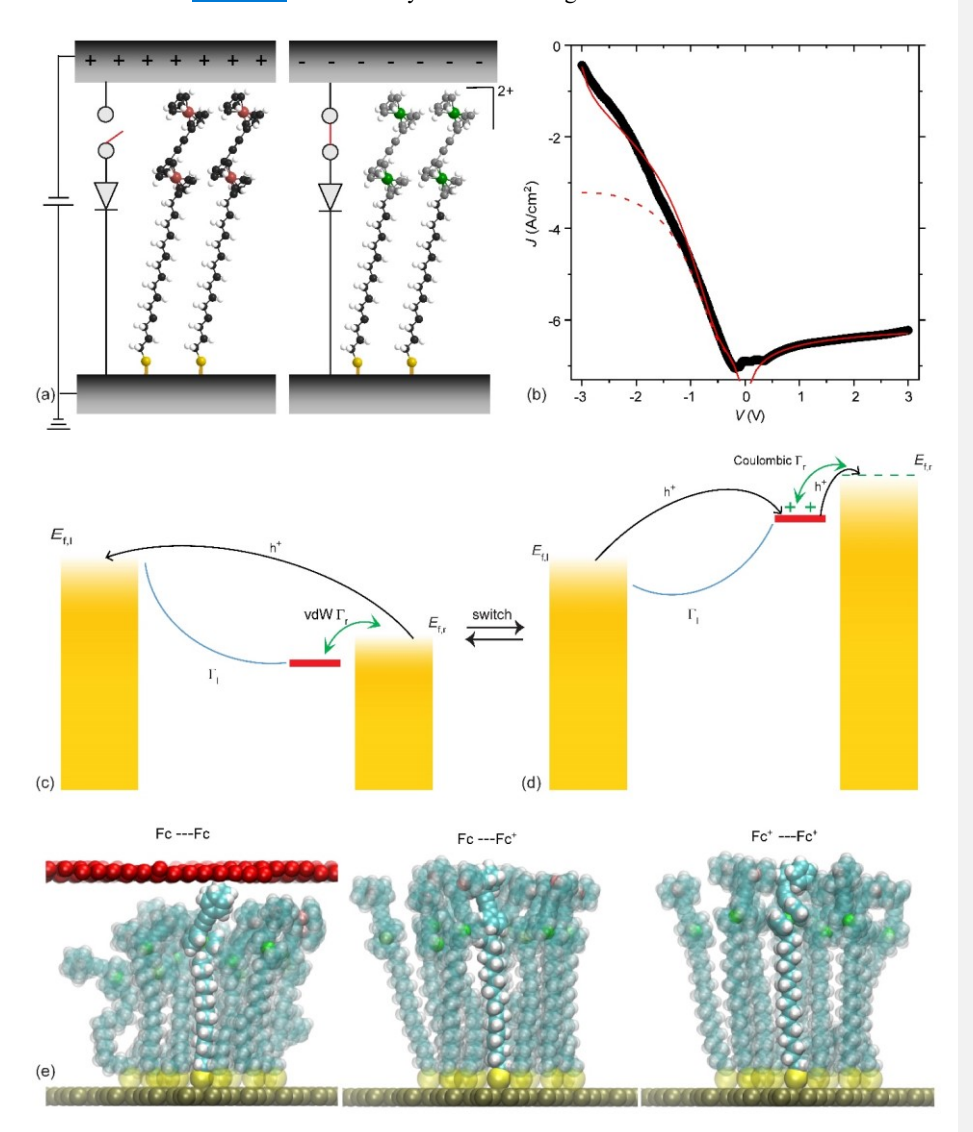


Figure 2: a) Schematic illustration of S(CH₁₅)Fc₂ inside a junction along with circuit symbols to indicate that this junction behaves as diode in series with an electrostatic on/off switch. b)

Average J(V) curve along with the predicted J(V) curve based on a single-level Landauer model (dashed line) and a fit to a modified Landauer model (solid red line) to account for electrostatic switching. Energy level diagrams of the off-state (c) and on-state (d) illustrating the operating mechanism as explained in the text (the filled states of the electrodes are indicated with the yellow rectangles) and the black arrows indicate change in the mechanism of charge transport. The green and blue arcs indicate Γ_1 and Γ_r and the increase in Γ_r results in broadening in the molecular level (red bar). Molecular dynamics simulations (e) showing electrostatic switching due to bias-induced electrostatic repulsion between the Fc₂ units and electrostatic attraction between the positively-charged Fc₂ units and the negatively charged top electrode (represented by the red oxygen atom spheres). Panel (a) is adapted from ref 5550, and panels (b) and (e) are reproduced with permission from ref 5247.

Table 1. Operating mechanisms of the dual-functional switches

| Junctiona | Function | Conduction | Switch | Change in | Diode | Change in |
|---|----------|--------------|----------------|---|--------------|---------------------------------|
| | | mechanism | mechanism | parameters ^b | mechanism | parameters ^b |
| M-S(CH ₁₅)Fc ₂ //M | Diode & | Change | Electrostatic | $\Gamma_{on} >> \Gamma_{of}$ | Asymmetric | $\eta = 0.95$ |
| | on/off | tunneling to | interactions | | voltage drop | |
| | switch | hopping | | | | |
| $M-S(CH_{11})MV^{2+}X^{2}//M$ | Diode & | Change | Dimerization & | Reduction in $E_{\rm HL}$ | Asymmetric | $\eta_{ m off} > \eta_{ m off}$ |
| | memory | tunneling to | ion migration | $\delta E_{\text{ME,on}} << \delta E_{\text{ME,off}}$ | voltage drop | |
| | | hopping | | $\Gamma_{on} \gg \Gamma_{off}$ | | |

^a M is the metal electrode, "-" indicates covalent contact and "//" indicates physisorbed contact.

Diode in series with memory switch. To obtain efficient on/off current switching, it is important to stabilize the charge injected in the molecule *in situ* (see next Section). To "lock" the charge on the molecule and to obtain stable on and off states, we replaced the Fc with methylviologen (MV²⁺) units and fabricated junctions with monolayers of S(CH₂)₁₁(MeV²⁺)X⁻2.⁵⁶ The counter ion X is typically a halide, and for this example we used $X = \Gamma$. Under wet electrochemical conditions, the dicationic MV²⁺ ground state is readily reduced to the radical cation MV^{*+} and it is well known that the MV^{*+} dimerizes to form a stable [MV^{*+}]₂ complex driven by π - π stacking and electron spin pairing with the two excess counter ions released into

Commented [D1]: Refs need to be updated

Formatted Table

^b All parameters are defined in Eq. 1 and Figs. 2c-d and 3c-d.

solution.^{57,58,59} In principle, dimerization and release of counter ions can stabilize the reduced form of MV in junctions resulting in large on/off conductance switching.

Figure 3a shows schematically the junctions with S(CH₂)₁₁(MeV²⁺)X⁻₂ in the ground state, and in the reduced form where [MV*+]2 dimers formed and the excess X- migrate to the bottom electrode (Table 1 summarizes all variables). Figure 3b shows the density functional theory (DFT) computed monolayer structures in both states which confirm that the dimer forms and X migrates to the bottom electrode. Figure 3c-d shows the operating mechanism. The LUMO centered on MV²⁺ only enters the bias window when negative bias is applied to the right electrode because the LUMO couples more strongly to $E_{f,r}$ than $E_{f,l}$ as it is separated from the left electrode by the long alkyl chain. At opposite bias no molecular frontier orbitals enter the bias window and hence this change in the mechanism of charge transport results in large current rectification (similar to the Fc diode explained above). Once the LUMO enters the bias window, an electron can be injected from $E_{f,r}$ into the LUMO resulting in formation of MV*+ followed by dimerization to [MV *+]2X-2. Since the right electrode is negatively biased, the two excess ions X⁻ readily migrate to the left electrode. This dimerization results in a reduction of the HOMO-LUMO energy gap, $E_{\rm H,L}$, and $\delta_{\rm EM}$ (double green arrows in Fig. 3c-d) so that the HOMO also enters the bias window which increases the conductance of the on-state even more. The high resistive state is associated with viologen in the dicationic MV²⁺ ground state where the mechanism of charge transport is off-resonant tunneling (black arrow in Fig. 2c), while the low resistive state is associated with viologen in [MV *+]2 dimer form with a small HOMO-LUMO gap and both the HOMO and LUMO involved in charge transport resulting in incoherent hopping (black arrows in Fig. 2d). In sharp contrast to the Fc-diodes discussed in the previous section, both dimerization and charge separation (by X- shuttling between molecule and electrode indicated with the single green arrow) provide the charge stabilization mechanisms to "lock" the molecules in two distinct resistive states resulting in large hysteresis in the J(V) curves (Table 1). While the alkyl chain structure below the bulky MV headgroups is sufficiently dynamic to allow small ions ($X^- = \text{halide}$) to readily migrate across the SAMs, the device performance is adversely affected with when large counterions ($X^- = \text{ClO}_4^-$ or PF₆) are used.

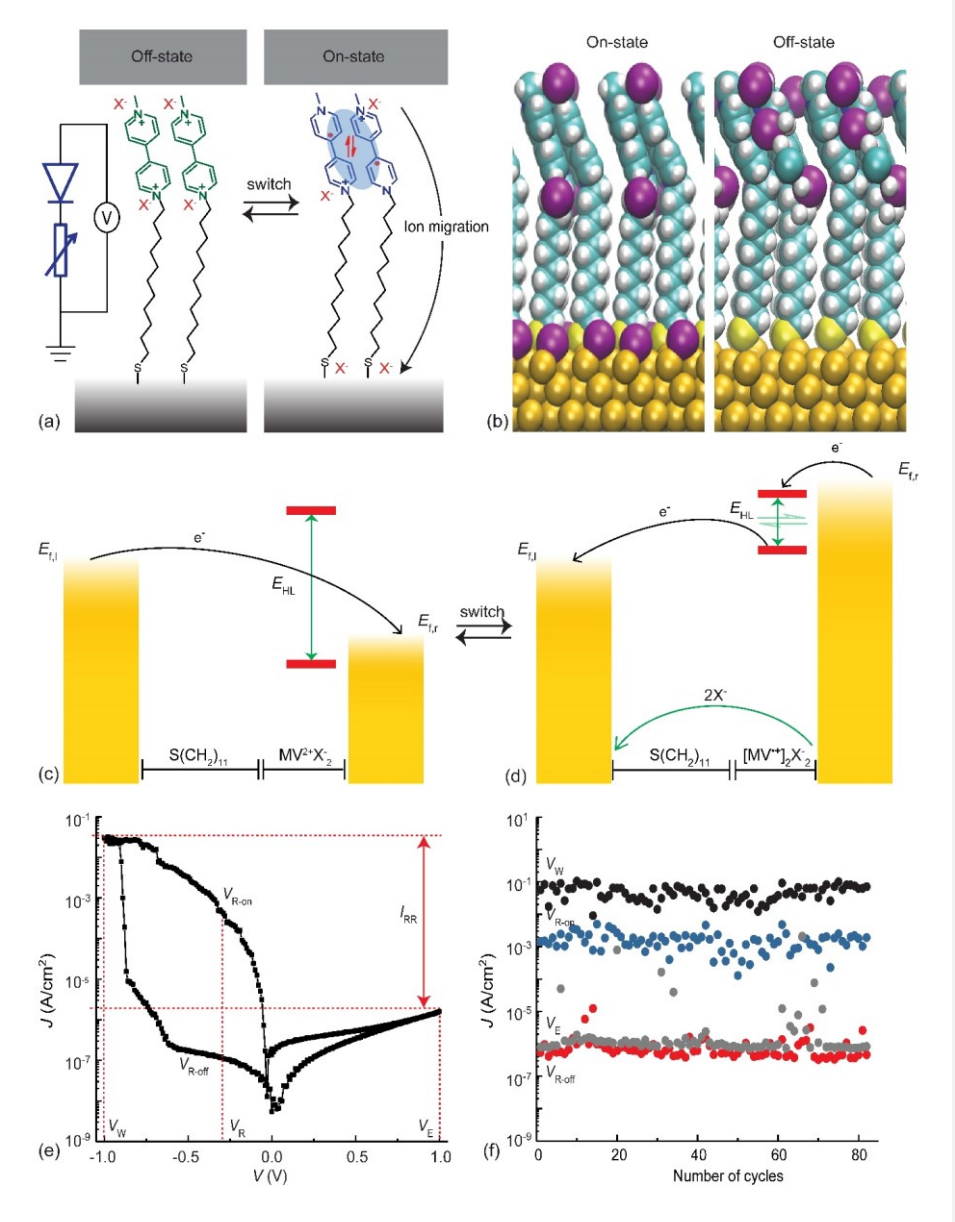


Figure 3: (a) Schematic illustration of the junction with a monolayer of $S(CH_2)_{11}MV^{2+}X_2^-$ at positive applied bias, and at negative applied bias when MV^{2+} is reduced to $[MV^{*+}]_2$. The blue shades indicate dimer formation. The black arrow indicates counter ion migration coupled with dimerization. The equivalent 1D-1R (1 diode and 1 variable resistor) circuit of the junction is shown on the right. (b) Periodic DFT calculations of $[MV^{*+}]_2$ SAM (on state) and MeV^{2+} SAM (off state) on Au. The counter ions are shown as purple spheres. Energy level diagrams showing the junctions in the off (c) and on state (d) summarizeing the switching mechanism as explained in the text (only the filled states of the electrodes are indicated with the yellow rectangles). The double green arrows indicate the change in E_{HL} and associated changes in δ_{EM} , the single green arrow indicates migration of X^- , and the black arrows indicate the change in the mechanism of charge transport. (e) Representative J(V) curve with low conductance (R_1) and high conductance (R_2) states labelled together with write (V_W), read (V_{OR} and V_{OR}) and erase voltages (V_E). (f) The output of 80 read-write-read-erase pulses (with $V_W = -1$ V, $V_E = +1$ V, $V_R = -0.3$ V) with R_1 (red), R_2 (blue), W (black), and E (grey) as a function of the number of cycles. Panels a, b, e and f are adapted from ref 56.

Figure 3e shows a typical J(V) curve with large unipolar hysteresis only at negative bias. The large current on/off ratio, $I_{\text{on/off}}$, of 6.7×10^3 and large RR of 2.5×10^4 show-prove that this junction combines the two functionalities of diode and variable resistor. Figure 3a shows the corresponding equivalent circuit which is the same of that of 1D-1R RRAM (1 diode 1 resistor resistive random access memory). To demonstrate 1D-1R RRAM functionality, we recorded write-read-erase-read (WRER) cycles using write voltage, $V_{\rm W}$, of -1.0 V, read voltage of -0.3 V to read out the on, $V_{\rm R,on}$, and off, $V_{\rm R,off}$, states, and erase voltage, $V_{\rm E}$, of +1.0 V, as input, as defined in Fig. 3e. Figure 3f shows the results where a junction was switched 80 times between the high conductance (on state) and low conductance (off state) states (which could

Commented [D2]: Ref needs to be updated

be extended to 2.0×10^6 voltage sweeps) and the junction retained the charge in the on and off states for 1.2×10^4 s (see ref 5651). From these results we conclude that the on/off states are stable during operation in high electric fields (~0.5 GV/m at 1 V).

Importance of charge locking. A major challenge is to stabilize the charge injected in the molecule in large electric fields of 0.1-1 GV/m that are typically required to obtain conductance switching in junctions. <u>IAlthough in 3-terminal</u> (electrochemical) molecular junctions, charge on the molecule can be stabilized with a gate electrode and switching can be observed, 60,61,62 but 2-terminal junctions lack a gate and the charge has to be stabilized by alternative means. For example, Fc-based diodes show only very marginal conductance switching with a small hysteresis in the J(V) curves of a factor 2-3.63 This small on/off ratio in the conductance between forward and backward bias sweeps is due to the lack of a charge stabilization mechanism: the charges readily hop on and off the Fc units at room temperature. Conductance switching based charge injection (or redox-events) in solid-state molecular junctions has also been observed for other types of redox groups, usually with low on/off ratios of <5.27,28,25,29 In general, in wet electrochemical environments the re-organization energies and so relative stabilities on the on and off states are larger than in solid state junctions due to counterion migration and reorganization of (many) solvent molecules. In solid-state junctions, however, these two mechanisms are usually not available and charges on the molecules are compensated by both image charges in the electrodes and inner sphere reorganization of the molecule resulting in low activation energies (which are often related to thermal broadening of the Fermi distributions of the leads). 4944,64,65,66,67,68,69 These energy differences are too small to prevent switching due to thermalization. Therefore, switching events are usually stochastic, as has been observed in junctions with, e.g., redox-active molecules or light-induced conformational switches, ^{25,31,32} preventing the use of such junctions in non-volatile memory applications.

In this context, the group of Chiechi reported an interesting approach to chemically lock two different conduction states of a light-triggered molecular switch in large area junctions. ⁷⁰ They formed junctions with sypiropyran which converts under the influence of light reversibly into the open-ring merocyanine isomer. At room temperature, merocyanine switches back to sypiropyran. By exposing the monolayer to acidic conditions, the merocyanine is protonated and stable enabling non-volatile memory, hence the on-state (with 10³ larger conductance than the off-state) is chemically "locked". This *ex situ* switching of monolayers, however, requires temporary removal of the top electrode (although Darwish *et al.* showed *in situ* "locking" of merocyanine by adding acid to the solution used in their break junction experiments ⁷¹). Others have reported control over binary switching by mechanically changing the electrode—electrode distance. ^{72,73} As a group, such approaches are not relevant for applications where electrodes have to be stationary.

Requirements for efficient switching. For the dual-functional switches to work well, the following criteria have to be fulfilled. i) The junction should operate in the intermediate/weak coupling regime. In the strong coupling regime coherent tunneling pathways dominate the mechanism of charge transport and charges are not injected in the molecules and thus the molecules cannot switch (apart from stochastic changes in conductance due to, *e.g.*, inelastic effects). ii) Charge injection should be coupled to an-in situ charge stabilization-mechanism, *i.e.*, charge locking mechanism, to prevent spontaneous switching back to the ground state. In other words, charge injection has to be coupled to a process that results in a switching event which, in turn, stabilizes the charged molecular state. Consequently, the mechanisms of charge transport have to be dominated by incoherent tunneling (*cf.* criterion i). iii) Two states should be available with different δ_{EM} and Γ resulting in a large change in the conductance and large change in energy level alignment of the junction to ensure control over two different functionalities.

Conclusions & Outlook. This overview introduces a molecular switch operable in the solid state leading to tunnel junctions with dual-functionality. The ability to perform multiple electrical transformation within a single molecular layer potentially reduces device complexity and power consumption. For instance, 1D-1R RRAM normally requires two junctions in series over each of which the potential drops. ⁷⁴ Consequently, operating voltages are high (2-6 V) and the fabrication of such devices typically involves complex multi-layered structures (5-7 layers) resulting in stacks with a thickness of 50-500 nm. 5654 In contrast, our junctions confine both functionalities within a single 2 nm thick molecular layer and operate <1.0 V, although scaling the lateral dimensions of molecular junctions is still both a scientific and technological challenge, and ie Industry device roadmaps vary widely between applications. For example, neuromorphic computing technologies require devices with high plasticity in sharp contrast with the highly static device requirements in CMOS-based technologies. However, device stability is always a key factor, and can be gauged in terms of, e.g., on/off state retention times, switching endurance and shelf-life. For instance, the S(CH₂)₁₁MV²⁺X⁻ switch has tested retention times of up to 1.2×10^4 s and an endurance of 2.0×10^6 voltage cycles, ⁵⁶ but metalthiolate bonds oxidise over time^{75,76} and can, in principle, be replaced with stable covalent bonds⁷⁷. Demonstrations of applications of molecular junctions in upcoming technologies (e.g., synaptic, neuromorphic, or soft robotic technologies 78,79) is an important future direction to pursue, in conjunction with scaling of switchable molecular junctions in commercially viable molecular platforms.80

The junctions introduced here are dynamic in nature (but this is true, at least to a certain degree, for all molecular junctions) and charge injection is coupled to conformational changes, changes in electrode—molecule interactions, image charge effects, migration of ions (if present) and associated electrostatic effects, and, therefore, it is important to study these kinds of dynamics in more detail to understand how they affect switching rates. Although the

examples introduced in this Progress Article changed from a low to a high conductance state, it would be very interesting to also design junctions that switches from a high to a low conductance state which could result, for example, in negative differential resistance. 81,82,83 Another interesting approach would be to couple electron transport to proton transport to induce charge locking. Proton coupled electron transport is already widely studied and involves reversible addition of hydride and associated formation of molecular bonds and changes in the electronic structure. 84,85,86 Likewise, other types of *in situ* chemical reactions could be explored to stabilize charges such as Brønsted 7 or bias induced Diels-Alder chemistry. 88 The switches introduced here also result in changes in the images charges in the electrodes, potential drops across the molecules and interfaces (especially when migrating counterions are involved) which currently have not been explored in detail. From the a computational point of view of predictive modelling, it is important to develop new methods to study changes in the energy level alignment in molecular junctions induced by the dynamics of the molecules and switching events.

${\bf Acknowledgements}$

We acknowledge the Ministry of Education (MOE) for supporting this research under award No. MOE2019-T2-1-137. Prime Minister's Office, Singapore under its Medium sized center program is also acknowledged for supporting this research. D.T. acknowledges support from Science Foundation Ireland (SFI) under awards number 15/CDA/3491 and 12/RC/2275. E.d.B. acknowledges support from the US National Science Foundation (grant no. ECCS#1916874).

Data Availability Statement

The data that support the findings of this study are available from the corresponding author upon reasonable request.

References

- ¹S. Ham, S. Choi, H. Cho, S.-I. Na and G. Wang Adv. Funct. Mater. **29**, 1806646 (2019).
- ²Y. van de Burgt, A. Melianas, S. T. Keene, G. Malliaras and A. Salleo, Nat. Electron. **1**, 386–397 (2018).
- ³E. J. Fuller, S. T. Keene, A. Melianas, Z. Wang, S. Agarwal, Y. Li, Y. Tuchman, C. D.
- James, M. J. Marinella, J. J. Yang, A. Salleo and A. Alec Talin Science 364, 570-574, (2019).
- ⁴J. Byun, Y. Lee, B. Lee, E. Oh, S. Chung, T. Lee, J. Cho, J. Kim and Y. Hong Sci. Robot. **3**, eaas9020 (2018).
- ⁵N. Xin, J. Guan, C. Zhou, X. Chen, C. Gu, Y. Li, M. A. Ratner, A. Nitzan, J. F. Stoddart and X. Guo Nat. Rev.s Phys. **1**, 211–230 (2019).
- ⁶P. Gehring, J. M. Thijssen, H. S. J. van der Zant Nat. Rev. Phys. 1, 381–396 (2019).
- ⁷H. Jeong, D. Kim, D. Xiang and T. Lee ACS Nano. **11**, 6511-6548 (2017).
- ⁸A. Vilan and D. Cahen Chem. Rev. **117**, 4248–4286 (2017).
- ⁹T. A. Su, M. Neupane, M. L. Steigerwald, L. Venkataraman and C. Nuckolls, Nat. Rev. Mater. 1, 16002 (2016).
- ¹⁰A. R. Garrigues, L. Wang, E. del Barco and C. A. Nijhuis Nat. Commun. 7, 11595 (2016).
- ¹¹A. R. Pease, J. O. Jeppesen, J. F. Stoddart, Y. Luo, C. P. Collier, J. R. Heat Acc. Chem. Res. 34, 433-444 (2001).
- ¹²B. L. Feringa, R. A. van Delden, N. Koumura, F. M. Geerstsema, E. M. Chem. Rev. **100**, 1789-1876 (2000).
- ¹³D. Bléger and S. Hecht. Angew. Chem. Int. Ed. **54**, 11338 11349 (2015).
- ¹⁴R. Klajn Chem. Soc. Rev. **43**, 148-184 (2014).
- ¹⁵B. L. Feringa Acc. Chem. Res. **34**,504-513 (2001).
- ¹⁶L. Bogani and W. Wernsdorfer Nat. Mater. 7, 179–186(2008).

¹⁷I. Ratera, and J. Veciana Chem. Soc. Rev. **138**, 303-349 (2012).

¹⁸C. Simão, M. Mas-Torrent, N. Crivillers, V. Lloveras 1, J. M.l Artés, P. Gorostiza, J.

Veciana and C. Rovira Nat. Chem. 3, 359-364 (2011).

¹⁹M. M. Russew, and S. Hecht Adv. Mater. **22**, 3348-3360 (2010).

²⁰G. de Ruiter and M. E van der Boom. J. Mater. Chem. **21**, 17575-17581 (2011).

²¹A. C. Aragonès, D. Aravena, J. I. Cerdá, Z. Acís-Castillo, H. Li, J. Antonio Real, F. Sanz,

J. Hihath, E. Ruiz and I. Díez-Pérez Nano Lett. 16, 218-226, (2016).

²²S. Erbas-Cakmak, D. A. Leigh, C. T. McTernan and A. L. Chem. Rev. 115, 10081-10206, (2015).

²³G. D. Harzmann, R. Frisenda, H. S. J. van der Zant and M. Mayor Angew. Chem. Int. Ed. 54, 13425 –13430 (2015).

²⁴S. J. van der Molen, J. Liao, T. Kudernac, J. S. Agustsson, L. Bernard, M. Calame, B. J. van Wees, B. L. Feringa, C. Schönenberger Nano Lett. **9**, 76-80, (2009).

²⁵L. Lörtscher, J. W. Ciszek, J. Tour and H. Riel Small **2**, 973–977 (2006).

²⁶A. J. Kronemeijer, H. B. Akkerman, T. Kudernac, B. J. van Wees, B. L. Feringa, P. W. M. Blom and B. de Boer Adv. Mater. **20**, 1467–1473 (2008).

²⁷J. Lee, H. Chang, S. Kim, G. Sook and H. Lee Angew. Chem. Int. Ed. **48**, 8501 –8504 (2009).

²⁸S. Seo, J. Lee, S. -Y. Choi and H. Lee J. Mater. Chem. **22**, 1868–1875 (2012).

²⁹Y. Li, M. Baghernejad, A. -G. Qusiy, D. Z. Manrique, G. Zhang, J. Hamill, Y. Fu, P.

Broekmann, W. Hong, T. Wandlowski, D. Zhang and C. Lambert Angew. Chem. Int. Ed. 54, 13586–13589 (2015).

³⁰J. M. Mativetsky, G. Pace, M. Elbing, M. A. Rampi, M. Mayor and P. Samorì J. Am. Chem. Soc. **130**, 9192-9193 (2008).

- ³¹F. Schwarz, G. Kastlunger, F. Lissel, C. Egler-Lucas, S. N. Semenov, K. Venkatesan, H. Berke, R. Stadler and E. Lörtscher Nat. Nanotechnol. **11**, 170, (2015).
- ³²C. Jia, A. Migliore, N. Xin, S. Huang, J. Wang, Q. Yang, S. Wang, H. Chen, D. Wang, B. Feng, Z. Liu, G. Zhang, D.-H. Qu, H. Tian, M. A. Ratner, H. Q. Xu, A. Nitzan and X. Guo Science **352**, 1443, (2016).
- ³³K. Voltz Curr. Opin. Struc. Biol. **18**, 106-111 (2008).
- ³⁴J. Zhou, K. Wang, B. Xu and Y. Dubi J. Am. Chem. Soc. **140**, 70–73 (2018).
- ³⁵P. Pourhossein, R. K. Vijayaraghavan, S, C. J. Meskers and R. C. Chiechi Nat. Commun. **7**, 11749 (2016).
- ³⁶M. Koole, J. M. Thijssen, H. Valkenier, J. C. Hummelen and H. S. J. van der Zant Nano Lett. **15**, 5569–5573 (2015).
- ³⁷H. Lissau, R. Frisenda, S. T. Olsen, M. Jevric, C. R. Parker, A. Kadziola, T. Hansen, H. S.J. van der Zant, M. B. Nielsen and K. V. Mikkelsen Nat. Commun. **6**, 10233 (2015).
- 38Y. –P. Zhang, L. –C. Chen, Z. –Q. Zhang, J. –J. Cao, C. Tang, J. Liu, L. –L. Duan, Y. Huo,
 X. Shao, W. Hong and H. –L. Zhang J. Am. Chem. Soc. 140, 6531–6535 (2018).
- ³⁹G. Ke, C. Duan, F. Huang and X. Guo InfoMat. **2**, 92–112 (2020).
- ⁴⁰E. Burzurí, A. García-Fuente, V. García-Suárez, K. S. Kumar, M. Ruben, J. Ferrer and H. S. J. van der Zant Nanoscale, 10, 7905 (2018).
- ⁴¹R. Hayakawa, M. A. Karimi, J. Wolf, T. Huhn, M. S. Zöllner, C. Herrmann and E. Scheer Nano Lett. 16, 4960-4967 (2016).
- ⁴²A. B. Allerman, P. W. M. Blom, D. M. de Leeuw and B. de Boer Nature **441**, 69–72(2006)
- ⁴³R. L. McCreery, H. Yan, A. J. Adam Phys. Chem. Chem. Phys. **15**, 1065 (2013).
- ⁴⁴A. P. Jauho, N. S. Wingreen and Y. Meir Phys. Rev. B **50**, 5528 (1994).
- ⁴⁵S. Datta Nanotechnology **15**, S433–S451 (2004).
- ⁴⁶ D. A. Egger, Z.-F. Liu, J. B. Neaton and L. Kronik Nano Lett. **15** 2448–2455 (2015).

- ⁴⁷ M. L. Perrin, C. J. O. Verzijl, C. A. Martin, A. J. Shaikh, R. Eelkema, J. H. van Esch, J. M. van Ruitenbeek, J. M. Thijssen, H.S. J. van der Zant and D. Dulić Nat. Nanotechnol. **8**, 282–287(2013).
- ⁴⁸L. Yuan, R. Breuer, L. Jiang, M. Schmittel and C. A. Nijhuis Nano Lett. 15, 5506–5512 (2015).
- ⁴⁹ X. Chen, H. V. Annadata, B. Kretz, M. Zharnikov, X. Chi, X. Yu, D. Egger and C. A. Nijhuis J. Phys. Chem. Lett. **10**, 4142-4147 (2019).
- ⁵⁰A. R. Garrigues, L. Yuan, L. Wang, E. R. Mucciolo, D. Thompson, E. del Barco and C. A. Nijhuis, Sci. Rep. **6**, 26517 **(2016).**
- ⁵¹A. Nitzan, M. Galperin, G. -L. Ingold and H. Grabert J. Chem. Phys. **117**, 10837-10841 (2002).
- ⁵²X. Chen, M. Roemer, L. Yuan, W. Du, D. Thompson, E. del Barco and C. A. Nijhuis, Nat. Nanotechnol. **12**, 797, (2017).
- ⁵³L. Yuan, L. Wang, A. R. Garrigues, L. Jian, H. V. Annadata, E. del Barco, and C. A. Nijhuis Nat. Nanotechnol. 13, 322-329 (2018).
- ⁵⁴D. Thompson and C. A. Nijhuis Acc. Chem. Res. **49**, 2061–2069 (2016).
- ⁵⁵N. Clement and A. Fujiwara Nat. Nanotechnol. **12**, 725–726 (2017).
- ⁵⁶Y. Han, C. Nickle, Z. Zhang, H. P.A.G. Astier, T. J. Duffin, D. Qi, Z. Wang, E. del Barco,
- D. Thompson and C. A. Nijhuis Nat. Mater. DOI: 10.1038/s41563-020-0697-5.
- ⁵⁷X. Tang, T. W. Schneider, J. W. Walker, and D. A. Buttry Langmuir **12**, 5921-5933 (1996).
- ⁵⁸D. W. Zhang, , J. Tian, , L. Chen, , L. Zhang, and Z. T. Li Chem. Asian J. **10**, 56-68, (2015).
- ⁵⁹B. Liu, A. Blaszczyk, M. Mayor and T. Wandlowski, ACS Nano. **5**, 5662-5672 (2011).
- ⁶⁰M. L. Perrin, E. Burzurí and H. S. J. Zant Chem. Soc. Rev. **44**, 902-919 (2015).

⁶¹H. Song, Y. Kim, Y. H. Jang, H. Jeong, M. A. Reed and T. Lee Nature **462**, 1039–1043 (2009).

⁶²X. Yin, Y. Zang, L. Zhu, J. Z. Low, Z. –F Liu, J. Cui, J. B. Neaton, L. Venkataraman and L. M. Campos Sci. Adv. 3, eaao2615 (2017).

⁶³C. A. Nijhuis, W. F. Reus and G. M. Whitesides J. Am. Chem. Soc. **131**, 17814-17827 (2009).

⁶⁴N. P. de Leon, W. Liang, Q. Gu and H. Park Nano Lett. **8**, 2963-2967 (2008).

⁶⁵A. Atxabal, T. Arnold, S. Parui, S. Hutsch, E. Zuccatti, R. Llopis, M. Cinchetti, F.

Casanova, F. Ortmann and L. E. Hueso Nat. Commun. 10, 2089 (2019).

⁶⁶A. R. Garrigues, L. Yuan, L. Wang, S. Singh, E. del Barco and C. A. Nijhuis Dalton Trans.
45, 17153-17159 (2016).

⁶⁷J. K. Sowa, J. A. Mol, C. A. D. Briggs and E. M. Gauger J. Chem. Phys. **149**, 154112 (2018).

⁶⁸J. O. Thomas, B. Limburg, J. K. Sowa, K. Willick, J. Baugh, G. A. D. Briggs, E. M. Gauger, H. L. Anderson and J. A. Mol Nat. Commun. 10, 4628 (2019).

⁶⁹M. Poot, E. Osorio, K. O'Neill, J. M. Thijssen, D. Vanmaekelbergh, C. A. van Walree, L. W. Jenneskens and Herre S. J. van der Zant Nano Lett. 5, 1031-1035 (2006).

⁷⁰S. Kumar, M. Merelli, W. Danowski, P. Rudolf, B. L. Feringa, and R. C. Chiechi Adv. Mater. 31, 1807831 (2019).

⁷¹N. Darwish, A. C. Aragonès, T. Darwish, S. Ciampi and I. Díez-Pérez Nano Lett. **14**, 7064–7070 (2014).

⁷²S. Y. Quek, M. Kamenetska, M. L. Steigerwald, H. J. Choi, S.G. Louie, M. S. Hybertsen, J. B. Neaton and L. Venkataraman Nat. Nanotechnol. 4, 230–234 (2009).

⁷³P. Moreno-García, A. La Rosa, V. Kolivoška, D. Bermejo, W. Hong, K. Yoshida, M. Baghernejad, S. Filippone, P. Broekmann, T. Wandlowski and N. Martín J. Am. Chem. Soc. 137, 2318–2327 (2015).

⁷⁴B. Cho, S. Song, Y. Ji, T. W. Kim and T. Lee Adv. Funct. Mater. **21**, 2806-2829 (2011).

⁷⁵J. C. Love, L. A. Estroff, J. K. Kriebel, R. G. Nuzzo and G. M. Whitesides Chem. Rev. **105**, 1103–1169 (2005).

⁷⁶S. O'Mahony, C. O'Dwyer, C. A. Nijhuis, J. C. Greer, A. J. Quinn and D. Thompson Langmuir **29**, 7271–7282 (2013).

⁷⁷Z. Liu, A. A. Yasseri, J. S. Lindsey, D. F. Bocian Science **302**, 1543-1545 (2003).

⁷⁸Q. Wan, M. T. Sharbati, J. R. Erickson, Y. Du, and F. Xiong Adv. Mater. Technol. 4, 1900037 (2019).

⁷⁹Y. J. Tan, H. Godaba, G. Chen, Si. T. M. Tan, G. Wan, G. Li, P. M. Lee, Y. Cai, S. Li, R. F. Shepherd, J. S. Ho and B. C. K. Tee Nat. Mater. **19**, 182-183 (2020).

⁸⁰A. J. Bergren, L. Zeer-Wanklyn, M. Semple, N. Pekas, B. Szeto and R. L. McCreery J. Phys.: Condens. Matter 28, 094011 (2016).

⁸¹A. Migliore and A. Nitzan ACS Nano **5**, 6669-6685 (2011).

⁸²S. Valianti and S. S. Skourtis J. Phys. Chem. B **123**, 9641–9653 (2019).

⁸³A. Migliore and A. Nitzan J. Am. Chem. Soc. **135**, 9420-9432 (2013).

⁸⁴C. D Bostick, S. Mukhopadhyay, I. Pecht, M. Sheves, D. Cahen and D. Lederman Rep. Prog. Phys. 81, 026601 (2018).

85S. Hammes-Schiffer J. Am. Chem. Soc. 137, 8860-8871 (2015).

⁸⁶M. H. V. Huynh and T. J. Meyer Chem. Rev. **107**, 5004-5064 (2007).

⁸⁷Y. Ai, A. Kovalchuk, X. Qiu, Y. Zhang, S. Kumar, X. Wang, M. Kühnel, K. Nørgaard and R. C. Chiechi Nano Lett. 18, 7552–7559 (2018). ⁸⁸A. C. Aragonès, N. L. haworth, N. Darwish, S. Ciampi, N. J. Bloomfield, G. G. Wallace, I. Díez-Pérez and M. L. Coote Nature 531, 88–91 (2016).